Seasonal speedup of a Greenland marine-terminating outlet glacier forced by surface melt–induced changes in subglacial hydrology

Seasonal speedup of a Greenland marine-terminating outlet glacier forced by surface melt–induced changes in subglacial hydrology

A. J. Sole,[1,2] D. W. F. Mair,[2] P. W. Nienow,[1] I. D. Bartholomew,[1] M. A. King,[3] M. J. Burke,[4] and I. Joughin[5]

Received 9 December 2010; revised 12 May 2011; accepted 23 May 2011; published 23 August 2011.

[1] We present subdaily ice flow measurements at four GPS sites between 36 and 72 km from the margin of a marine-terminating Greenland outlet glacier spanning the 2009 melt season. Our data show that >35 km from the margin, seasonal and shorter–time scale ice flow variations are controlled by surface melt–induced changes in subglacial hydrology. Following the onset of melting at each site, ice motion increased above background for up to 2 months with resultant up-glacier migration of both the onset and peak of acceleration. Later in our survey, ice flow at all sites decreased to below background. Multiple 1 to 15 day speedups increased ice motion by up to 40% above background. These events were typically accompanied by uplift and coincided with enhanced surface melt or lake drainage. Our results indicate that the subglacial drainage system evolved through the season with efficient drainage extending to at least 48 km inland during the melt season. While we can explain our observations with reference to evolution of the glacier drainage system, the net effect of the summer speed variations on annual motion is small (~1%). This, in part, is because the speedups are compensated for by slowdowns beneath background associated with the establishment of an efficient subglacial drainage system. In addition, the speedups are less pronounced in comparison to land-terminating systems. Our results reveal similarities between the inland ice flow response of Greenland marine- and land-terminating outlet glaciers.

Citation: Sole, A. J., D. W. F. Mair, P. W. Nienow, I. D. Bartholomew, M. A. King, M. J. Burke, and I. Joughin (2011), Seasonal speedup of a Greenland marine-terminating outlet glacier forced by surface melt–induced changes in subglacial hydrology, *J. Geophys. Res.*, *116*, F03014, doi:10.1029/2010JF001948.

1. Introduction

[2] The Greenland Ice Sheet (GRIS), which contains sufficient water equivalent to raise global sea level by ~7 m [*Lemke et al.*, 2007], has experienced increased rates of mass loss over the last decade due to increased surface melt and runoff [*Tedesco*, 2007; *Tedesco et al.*, 2008; *van den Broeke et al.*, 2009] and accelerated ice discharge [*Rignot and Kanagaratnam*, 2006; *Rignot et al.*, 2008; *Pritchard et al.*, 2009]. Approximately half the current mass loss is through melt and runoff, while the remainder is due to ice discharge to the surrounding oceans [*Shepherd and Wingham*, 2007; *van den Broeke et al.*, 2009]. Two principal mechanisms by which climate could influence ice discharge have been proposed: (1) ice geometry and thickness changes at the calving fronts of marine-terminating glaciers reduce resistive forces, resulting in glacier acceleration and thinning or "drawdown" [*Thomas*, 2004; *Howat et al.*, 2005; *Luckman and Murray*, 2005; *Howat et al.*, 2007; *Nick et al.*, 2009], and (2) increased surface melt reaches the ice sheet bed locally, [*Das et al.*, 2008] enhancing basal sliding and lowering the ice sheet surface, exposing it to higher melt rates [*Zwally et al.*, 2002]. Although both effects have been modeled for individual glacier basins [e.g., *Price et al.*, 2008; *Pimentel and Flowers*, 2010; *Nick et al.*, 2009], their relative importance for the mass balance of the whole GRIS is at present unknown because continental-scale ice sheet models do not include the necessary physics to represent them [e.g., *Parizek and Alley*, 2004; *Huybrechts et al.*, 2004].

[3] The drainage of surface lakes to the bed via hydrofracture [*van der Veen*, 2007] enables subsequent rapid routing of surface melt to the glacier base [*Shepherd et al.*, 2009] and causes short-lived ice acceleration [*Das et al.*, 2008]. Acceleration is driven by a reduction in effective pressure, which promotes basal sliding at times when the

[1]School of Geosciences, University of Edinburgh, Edinburgh, UK.
[2]School of Geosciences, University of Aberdeen, Aberdeen, UK.
[3]School of Civil Engineering and Geosciences, Newcastle University, Newcastle upon Tyne, UK.
[4]Department of Geography, Simon Fraser University, Burnaby, British Columbia, Canada.
[5]Applied Physics Laboratory, University of Washington, Seattle, Washington, USA.

0148-0227/11/2010JF001948

input of surface meltwater to the bed exceeds the capacity of the subglacial drainage system [*Iken*, 1981; *Iken and Bindschadler*, 1986; *Kamb*, 1987; *Meier et al.*, 1994; *Anderson et al.*, 2004]. Following the establishment of local surface to bed conduits, land-terminating margins have been shown to respond rapidly to seasonal [*Bartholomew et al.*, 2010] and diurnal [*Shepherd et al.*, 2009] variations in surface meltwater generation with the net effect of increasing annual ice speed [*Joughin et al.*, 2008a; *Bartholomew et al.*, 2010]. A 17 year record from west Greenland found a weak negative correlation between ice speed and melting [*van de Wal et al.*, 2008], suggesting that in certain situations, other processes such as changing ice geometry might eclipse the importance of basal sliding. Inland expansion of the region experiencing melting, expected in a warming climate, will increase the area over which seasonal acceleration occurs and, thus, its potential impact on annual ice flux [*Sundal et al.*, 2009]. A positive relationship between surface melting and ice speed is important because it would initiate a positive feedback whereby in a warmer climate ice would flow increasingly quickly into the lower-elevation ablation area, thereby experiencing higher melt rates.

[4] In contrast, marine-terminating GRIS outlet glaciers have generally displayed less sensitivity to variations in meltwater forcing [*Echelmeyer and Harrison*, 1990; *Joughin et al.*, 2008a]. Instead, seasonal flow variations at such glaciers have been explained by changes in calving rate due to the breakup of the seasonal ice mélange (a mixture of fjord sea ice and recently calved ice) [*Joughin et al.*, 2008b; *Amundson et al.*, 2010] or the ungrounding of ice near the terminus [*Howat et al.*, 2007]. However, most observations of seasonal flow variations on GRIS marine-terminating glaciers come from close to their termini (<30 km) where calving is very likely to be the principal control on ice flow [*Joughin et al.*, 2008b]. On the other hand, a "minisurge" of Ryder Gletscher in northern Greenland, which experienced a 400% speedup over a 7 week period toward the end of the 1995 melt season, was likely related to changes in subglacial water pressure caused by the drainage of several large supraglacial lakes [*Joughin et al.*, 1996]. Similarly, *Andersen et al.* [2010] found a correlation (with a 1 day lag) between modeled surface melting and ice speed at Helheim Gletscher, east Greenland. The relationship was strongest for the heavily crevassed terminus region, but variations in flow were small compared to those attributed to calving front changes. *Howat et al.* [2010] found that close to the calving fronts of several marine-terminating outlet glaciers in west Greenland, ice speed decreased by 40% to 60% following the drainage of surface lakes in midsummer. Furthermore, subglacial hydrology has been shown to exert a strong control on the dynamics of large marine-terminating glaciers in Alaska [e.g., *Kamb et al.*, 1994; *O'Neel et al.*, 2001]. The relative importance of calving and subglacial hydrology on controlling ice flow of GRIS marine-terminating glaciers farther inland from their termini is not known. There is, therefore, a clear need to include both empirically constrained representations of basal hydrology and the long- and short-term effects of ice front changes and their transmission inland into models which aim to predict the future contribution of the GRIS to global sea level rise.

[5] Here we present subdaily ice flow measurements from Global Positioning System (GPS) sites located between 36 and 72 km from the calving front of a major marine-terminating GRIS outlet glacier spanning the 2009 melt season (May to August). These data show that far into the ice sheet interior, seasonal and shorter-term variations in ice flow are principally controlled by surface melt–induced changes in subglacial hydrology rather than by changes at the calving front.

2. Field Site and Methods

[6] Kangiata Nunata Sermia (KNS) is a large tidewater outlet glacier which terminates at the head of the ~175 km long Nuup Kangerlua Fjord in southwest Greenland at ~64.30°N (Figure 1a). The glacier, which flows at ~6000 m yr^{-1} at its calving front [*Joughin et al.*, 2010], drains an area of ~31,400 km^2 (see Figure 1c) toward a ~4.5 km wide calving front. KNS accelerated by 27% between 2000 and 2005 and retreated by 580 m between 2006 and 2007 [*Rignot and Kanagaratnam*, 2006; *Moon and Joughin*, 2008; *Joughin et al.*, 2010]. Surface lowering rates exceeded 10 m yr^{-1} between 1998 and 2001 within 10 km of the glacier's calving front and decreased to approximately zero 30 km inland [*Thomas et al.*, 2009] (Figure 1b).

[7] On 11 May (day 131), prior to the onset of runoff in 2009, four dual-frequency GPS receivers ("rovers") were deployed on a single flow line of KNS at sites 36 km (KNS1), 48 km (KNS2), 59 km (KNS3), and 72 km (KNS4) from the KNS calving front (Figure 1a and Table 1). Extensive crevassing precluded deploying GPS receivers closer to the terminus. Each on-ice GPS antenna was mounted on a support pole drilled into the ice (to 5 m depth for KNS1 and KNS2 and to 3 m depth for KNS3 and KNS4), which froze in place subsequently, providing measurements of ice motion that were independent of ablation. None of the poles tilted significantly during the survey period. A fifth GPS receiver acted as a reference station and was installed on bedrock overlooking the calving front of KNS. The maximum baseline between reference station and rover was ~70 km. The GPS data were sampled and recorded at 10 s intervals, with a continuous record obtained from 11 May (day 131) to 13 August (day 225) for KNS1 and to 23 August (day 235) for KNS2, KNS3, and KNS4. The data were processed in Track v1.21 [*Chen*, 1998; *Herring et al.*, 2010] relative to the off-ice reference station using a kinematic approach [see *King*, 2004] that utilized International Global Navigation Satellite Systems Service (IGS) precise orbits and loosely constrained site motion to be no more than 0.02 m per epoch. We estimated relative (base to rover) tropospheric zenith delay parameters which, if not estimated, could result in biased height time series. Site coordinates were produced for each measurement epoch, and these were then rotated to along- and across-flow directions, from which speeds were computed. Daily horizontal speeds were calculated by taking the difference of 1 h mean positions every 24 h. Uncertainties associated with mean hourly positioning are <0.5 cm in the horizontal and <1 cm in the vertical, corresponding to annual horizontal speed uncertainties of <3.7 m yr^{-1}. The determined vertical positions were detrended by removing a linear component assumed to represent bed-parallel motion to give residual vertical displacement, which includes horizontal (and ver-

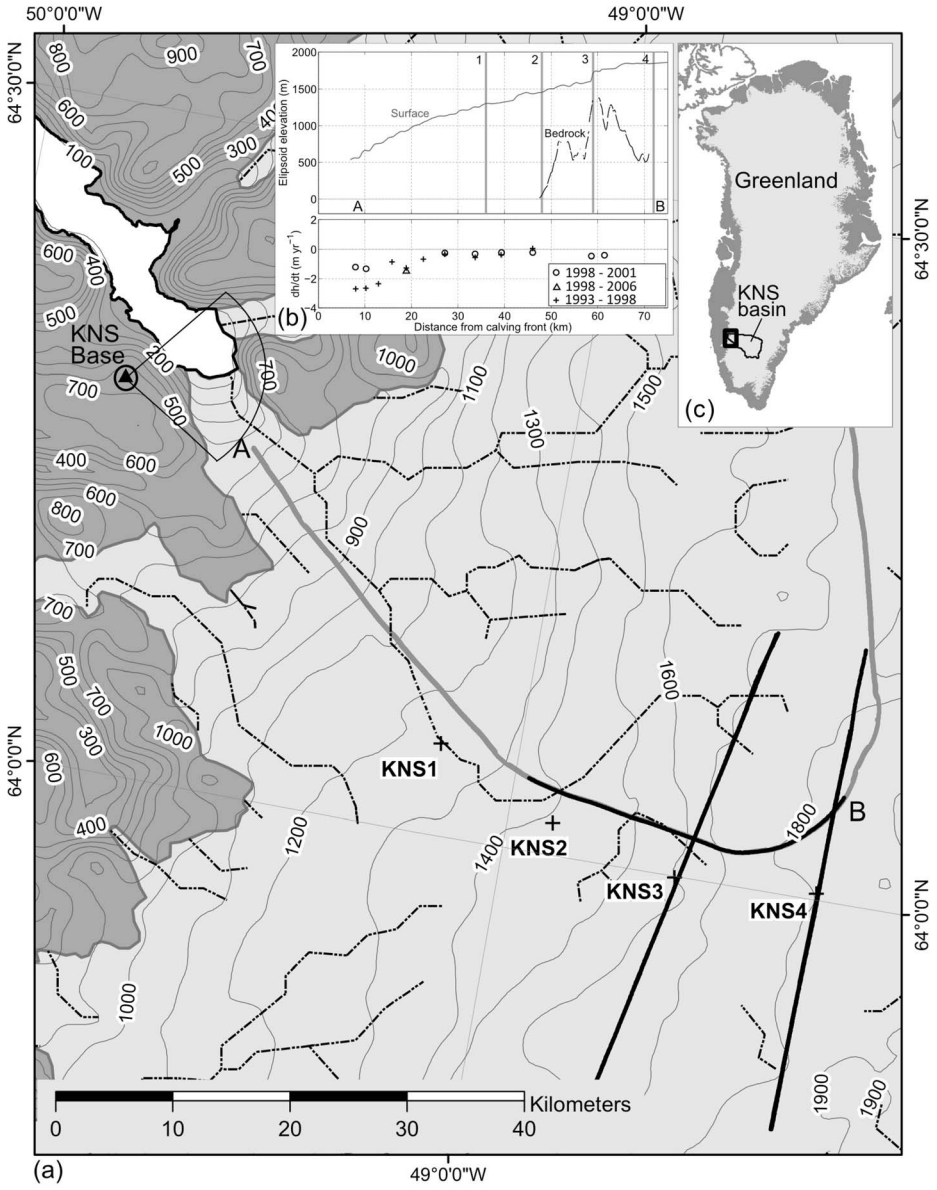

Figure 1. (a) Location of KNS and the GPS transect. GPS sites KNS1–KNS4 are represented as black crosses. Bold black lines show airborne radio echo sounding transects of bed topography, and the bold gray line shows the laser altimetry flight line for ice surface topography. Contours show ice sheet elevation above the geoid (m), and dot-dashed lines represent surface (and approximate subglacial) hydrological pathways. The location of the off-ice reference station (KNS Base) and time-lapse camera approximate field of view are also shown. (b) Bed and surface topography for KNS centerline (A–B) as well as surface elevation change rates for the along-flow flight line shown in Figure 1. (c) The location of the KNS surface drainage basin.

tical) strain rate as well as bed separation and till dilation [*Howat et al.*, 2008].

[8] At each GPS site, snow depth was measured before the onset of runoff, and mean surface lowering rate and air temperature were measured every 15 min using a Campbell SR50A ultrasonic depth gauge and a Campbell T107 shielded temperature sensor, respectively. The surface lowering data, combined with appropriate densities of snow and firn facies [*Parry et al.*, 2007], were used to estimate the potential water input to the subglacial drainage system. We

Table 1. GPS Site Characteristics

	Distance From Calving Front (km)	Elevation Above Geoid (m)	Approximate Ice Thickness (m)
KNS1	36	1282	unknown
KNS2	48	1443	1500
KNS3	59	1648	350
KNS4	72	1840	1200

Figure 2. Time-lapse images of (a) early season with fjord ice mélange intact, 12 May, day 132; (b) the breakup of seasonal fjord ice mélange, 4 June, day 155; (c) when a small ice-free area and turbid plume first became visible in the fjord at the KNS terminus, 11 July, day 192; and (d) when the ice-free area and turbid plume expanded significantly, 14 July, day 195.

acknowledge that initial snowmelt is likely to refreeze in the snowpack [*Pfeffer et al.*, 1991] but assume that the majority of measured surface lowering represents melting ice which does produce runoff. A time-lapse camera system was installed adjacent to the off-ice reference station with a field of view encompassing the calving terminus of KNS (Figure 1a) and obtained hourly photographs over the entire melt season (Figure 2). The resulting photographs allowed a qualitative analysis of water outflow from the glacier system [e.g., *O'Neel et al.*, 2001] and the timing of the ice mélange breakup.

[9] Supraglacial lake evolution was analyzed using Moderate Resolution Imaging Spectroradiometer (MODIS) level 1B calibrated radiances (MOD02QKM) of the catchment, which were corrected for atmospheric effects and orthorectified using the *Gumley et al.* [2007] method after *Sundal et al.* [2009]. Forty-seven MODIS images were used spanning the period 30 April to 27 August, representing all days when lake identification was not impeded by cloud cover. Band 3 data were upsampled from 500 to 250 m resolution using a resolution-sharpening algorithm [*Gumley et al.*, 2007] which bilinearly interpolates band 3 to the equivalent of 250 m resolution [*Sundal et al.*, 2009]. Supraglacial lakes were identified using membership functions of the ratio of band 1 to band 3 and band 1 radiances (band 1/(band 1 + band 3)) [*Sundal et al.*, 2009], and their areas (A) were subsequently calculated. Comparison between areas for 45 lakes automatically identified on three 250 m pixel size MODIS images and manually digitized on three concurrent 14 m pixel size Landsat images (days 173, 198, and 230) gives a correlation of 0.84 ($p < 0.05$) with a 1σ uncertainty (A_{err}) of 0.2 km^2 per lake. This is comparable

with the 1σ uncertainty of 0.22 km^2 per lake from a comparison of MODIS-derived and Advanced Spaceborne Thermal Emission and Reflection Radiometer (ASTER)–derived (15 m pixel size) lake areas from a similar region of the ice sheet [*Sundal et al.*, 2009]. Mean lake depths (D) were estimated from their relationship with band 1 reflectance after *Box and Ski* [2007],

$$D = \frac{0.716738}{(R + 0.036304)} + 0.701691, \quad (1)$$

where R is band 1 reflectance. This relationship has 1σ uncertainty D_{err} of 0.86 m [*Box and Ski*, 2007]. Lake volume V was simply estimated by multiplying D by A. The uncertainty V_{err} associated with estimating V for a single lake is therefore

$$V_{\mathrm{err}} = \left[\sqrt{\left(\frac{D_{\mathrm{err}}}{D}\right)^2 + \left(\frac{A_{\mathrm{err}}}{A}\right)^2}\right] V. \quad (2)$$

[10] We used the ASTER Global Digital Elevation Model (GDEM, http://www.ersdac.or.jp/GDEM/E/2.html) combined with the *Bamber et al.* [2001] 1 km resolution Digital Elevation Model (DEM, which has an accuracy of −0.33 ± 6.97 m for slopes 0.0° to 1°) farther inland to estimate the extent of KNS's surface drainage basin. Water at the ice sheet base is expected to flow normal to equipotential contours which, because of the density difference between water and ice, can be expected to be 11 times more sensitive to ice surface slope than bedrock slope [*Shreve*, 1972]. Despite this, it is possible that at several locations along our transect (see Figure 1b), bed topography is sufficiently steep to control subglacial water routing. However, there are no ice-marginal rivers large enough to evacuate runoff from the KNS basin visible in satellite imagery of the KNS margin, and so we assume the majority of runoff is injected directly into the Nuup Kangerlua Fjord. Therefore, in the absence of more extensive or accurate bed data, we also used the surface topography data to delineate the extent and likely flow paths of theoretical subglacial drainage (Figure 1).

3. Results

3.1. Horizontal Motion

[11] At the start of our survey period all the sites were flowing at steady background speeds (Figures 3a–3d). In the absence of GPS data spanning a winter season, background speed for each site was estimated by taking a mean early season value, prior to the start of melting and the breakup of the ice mélange. Following the onset of melting at each site, ice flow rate increased above background with a resultant up-glacier evolution of both the onset and peak of speed enhancement (Figures 3a–3d). Seasonal acceleration at KNS1, KNS2, KNS3, and KNS4 began on approximately days 156, 183, 190, and 198, respectively. Ice flow rate reached a maximum at KNS1 on day 191 (535 m yr^{-1}, 40% above background), at KNS2 on day 203 (271 m yr^{-1}, 25% above background), and at both KNS3 and KNS4 on day 213 (200 and 133 m yr^{-1}, 15% and 36% above background speed, respectively). Initially, at each site the acceleration was small (giving speeds generally <10% above background) but increased episodically toward a peak. After this, speeds varied considerably but gradually returned to values below or similar to background.

[12] Superimposed on the seasonal ice flow pattern were multiple short-lived speedup events lasting 1 to 15 days, some of which occurred at multiple sites. For the remainder of the paper, we refer to six of the more significant individual speedup events as S1 (days 156–170), S2 (days 177–184), S3 (days 189–195), S4 (days 201–204), S5 (days 212–214), and S6 (days 220–223) since these are synchronous across multiple sites (Figures 3a–3d). For example, during S3, the largest of these events at KNS1, speed increased by 33% of background (from 408 to 535 m yr^{-1}) in 3 days. At the same time at KNS2, speed increased from 221 to 259 m yr^{-1} (20%), while KNS3 accelerated from 174 to 183 m yr^{-1} (6%). There was no discernible concurrent speedup at KNS4.

[13] Following S4 at KNS1, ice flow decreased to consistently >6% below background for 9 days, while at KNS2 speed decreased to >1% below background for 5 days. This period of below-background flow was interrupted at both sites by S5, during which speed increased to 2% and 4% above background at KNS1 and KNS2, respectively. Immediately after S6, speeds at KNS2 decreased steadily, reaching a minimum of ~6% below background after 11 days, while at KNS1, speed decreased to ~10% below background over 3 days. A similar pattern of speedup followed by slowdown to below background speeds was also observed at KNS3 and KNS4. By the end of our survey, speeds at both KNS1 and KNS2 were ~5% below background, while at KNS3 and KNS4 speeds were 1% and 2% below their background values, respectively.

3.2. Vertical Motion

[14] At KNS1, the ice surface was raised by between 0.025 ± 0.01 and 0.140 ± 0.01 m coincident with these short-lived speedup events. During each event at KNS1, maximum horizontal speed coincided with maximum rate of vertical uplift rather than peak vertical displacement (e.g., day 191, Figure 3a). Indeed, for the whole survey period, horizontal ice speed is more strongly correlated with rate of vertical displacement ($r = 0.72$ and $p < 0.05$) than it is with vertical displacement itself ($r = 0.42$ and $p > 0.05$). After each speedup event, the ice surface subsided, at times (e.g., days 173–178 and days 205–212) to levels below those immediately prior to the speedup. The rate of subsidence was generally less than the rate of uplift (e.g., uplift of ~0.06 cm d^{-1} from days 155–160 and subsidence of ~0.02 cm d^{-1} from days 160–178). Sites KNS2–KNS4 showed smaller magnitude variations in vertical position, but maximum horizontal speed did not always coincide with maximum rate of vertical uplift (Figures 3b–3d).

3.3. Calving Front Changes

[15] The breakup of the seasonal ice mélange occurred on day 155 (vertical solid black line in Figures 3a–3f; compare Figures 2a and 2c), a day before the onset of seasonal acceleration at KNS1. A turbid plume first appeared in the time-lapse photographs on day 192 (vertical black dotted line in Figures 3a–3f), 1 day after maximum speed at KNS1. The plume grew dramatically on day 195 (vertical black dashed line in Figures 3a–3f), flushing remnant sea ice and

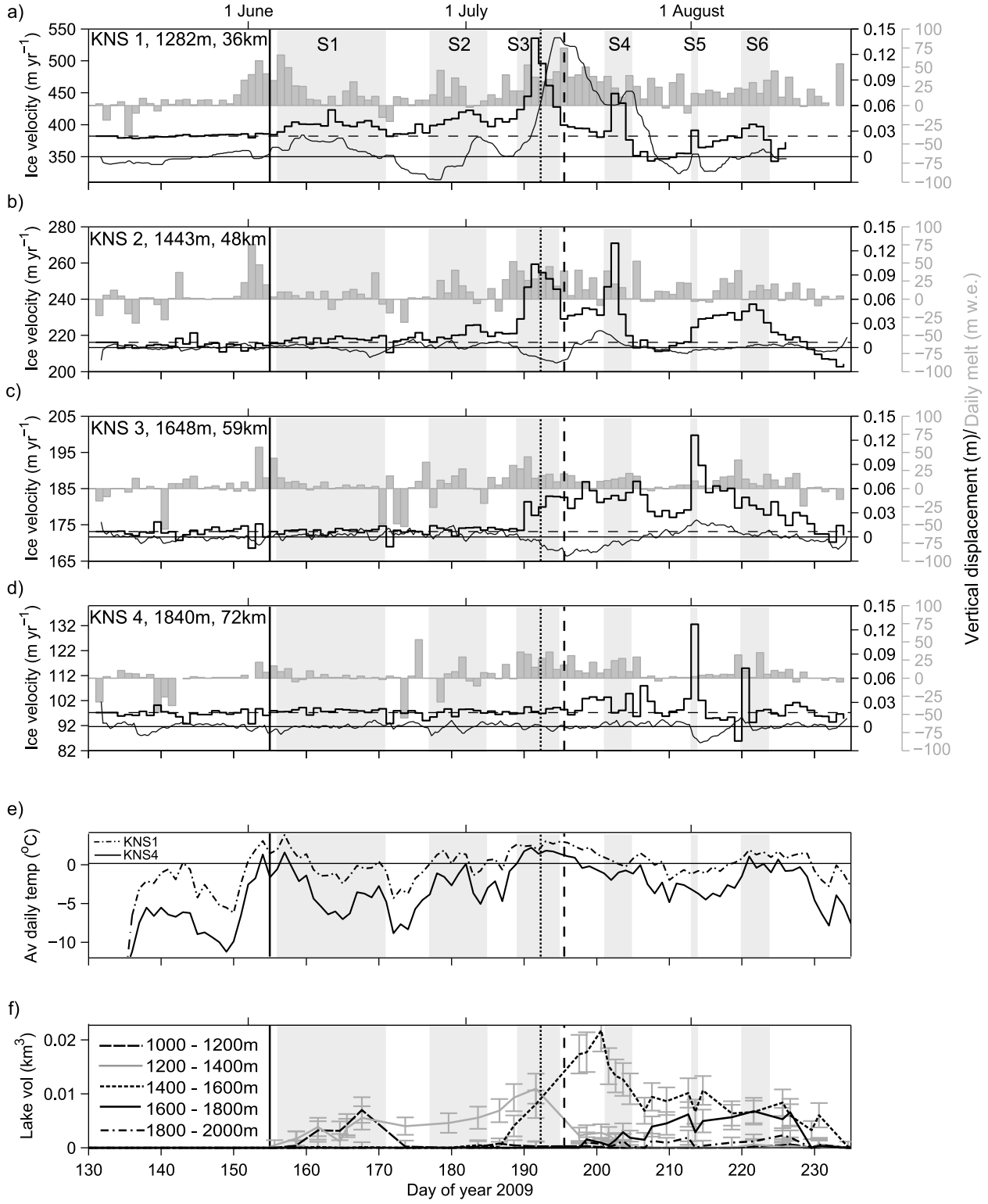

Figure 3. (a–d) Daily horizontal speed (stepped line), 6 hourly vertical displacement (smooth line), and daily water equivalent ice melt (gray bars) at KNS1–KNS4. The horizontal dashed lines represent respective background speeds, and shaded light gray areas display periods categorized as short-lived speedup events (S1–S6). (e) Daily mean temperature for KNS1 and KNS4. (f) Lake volume by 200 m elevation band derived from MODIS imagery and the relationship between radiance and lake depth from *Box and Ski* [2007]. The solid vertical black line in each plot shows the timing of the breakup of seasonal fjord ice mélange (day 155, 4 June), the dotted black vertical line indicates when a small ice-free area and turbid plume first became visible in the fjord at the KNS terminus (day 192, 11 July), and the dashed vertical black line shows when the ice-free area and turbid plume expanded significantly (day 195, 14 July).

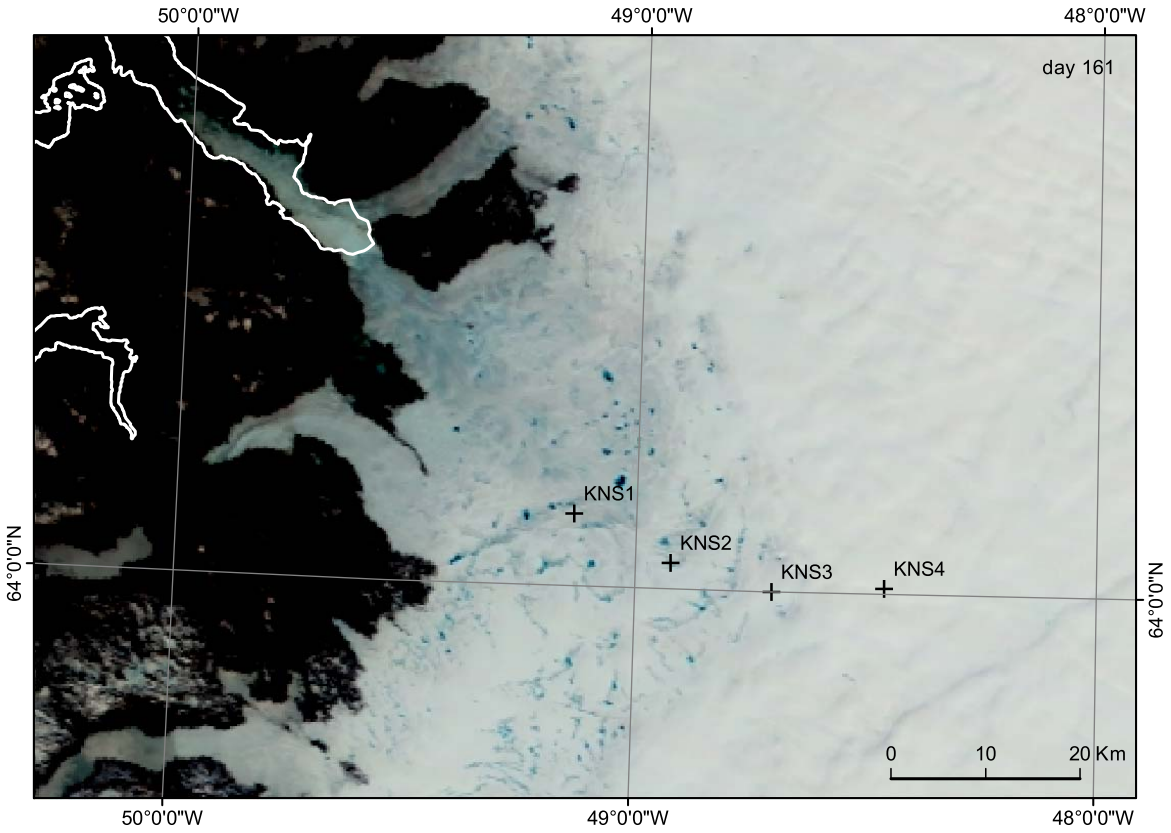

Figure 4. Example of a MODIS image showing surface lakes (dark blue on-ice patches) on 10 June, day 161.

recently calved glacier ice down fjord (Figure 2d). The plume persisted until day 209, after which it returned only sporadically. According to the time-lapse images, after the initial mélange breakup the calving front remained in approximately the same position for the entirety of our survey period.

3.4. Supraglacial Lake Drainage

[16] Surface lakes are clearly visible in MODIS imagery (e.g., Figure 4) of KNS from day 155, 2 days before the start of S1. MODIS imagery has a horizontal resolution of 0.25 by 0.25 km, and so all of the visible lakes (assuming a conical bathymetry [*Krawczynski et al.*, 2009] with a diameter-to-depth aspect ratio of 100:1 [e.g., *Sneed and Hamilton*, 2007; *Krawczynski et al.*, 2009]) contain sufficient water ($\sim 2 \times 10^{-5}$ km^3) to force hydrofracture through 1000 m of ice [*Krawczynski et al.*, 2009]. Figure 3f shows a time series of supraglacial lake volume for 200 m elevation bands within the KNS catchment with error bars for the 1σ uncertainty. The region with the greatest lake volume migrates up glacier through the season. The expansion of lake area within each elevation band is controlled by surface melting. Rapid decrease in lake area corresponds to lake drainage, probably initiated by hydrofracturing once sufficient water has gathered [*Krawczynski et al.*, 2009]. The largest of these drainage events within each elevation band coincide with the largest accelerations at the respective GPS sites but also affect adjacent sites. For example, the biggest 1200–1400 m lake drainage event (days 192–197) coincided with the biggest speedup (S3) at KNS1 and with S3 at KNS2. Similarly, the biggest 1400–1600 m lake drainage event (days 201–207) coincided with the biggest speedup (S4) at KNS2 and also with S4 at KNS1.

[17] Several lakes drained between days 201 and 205 coinciding with S4, the peak ice speed at KNS2. According to the surface (and by extension, bed) flow routing (dot-dashed lines in Figure 1a), these lakes are <8 km upstream of KNS2. The first lake (L1 at ~1500 m) drained over a 3 day period from day 200 to day 203 (Figures 5b and 5c). A second lake (L2 at ~1300 m) drained from day 201 to day 206, and several other up-glacier lakes (L3–L7 between ~1450 and 1650 m) decreased in size between days 204 and 207 but did not completely empty (Figure 5a). A time series of the combined discharge from L1 and L2 (and subsequent surface melt from these lake drainage basins) was estimated by linearly interpolating the reductions in MODIS-derived [*Box and Ski*, 2007] L1 and L2 volume through time (Figures 5b and 5c). The initiation of these lake drainages preceded the onset of S4 at KNS1 and KNS2 by approximately 24 h.

4. Discussion

[18] The synchroneity of the short-lived speedups at different sites suggests a common forcing which acts over length scales of at least ~11 km. There are two mechanisms that could be responsible for the observed synchronous behavior: (1) changes at the calving front could propagate

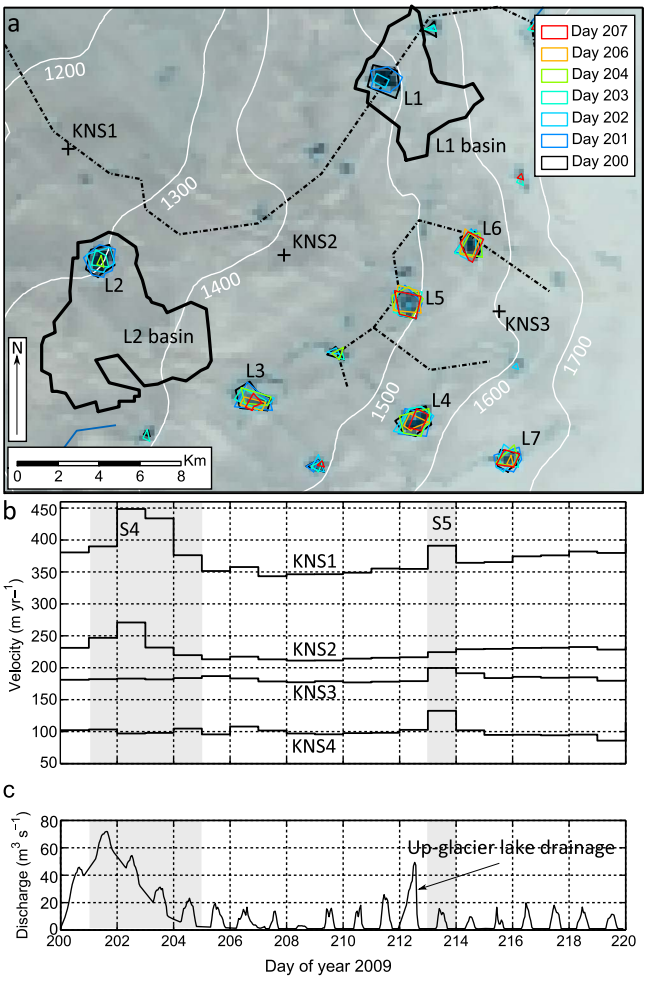

Figure 5. (a) Changes in lake area during S4. Dot-dashed black lines represent supraglacial or subglacial flow pathways, thick black lines delineate L1 and L2 drainage basins, and colored polygons show daily lake area. The GPS sites are marked with black crosses. (b) Daily horizontal surface speed and (c) combined discharge of lakes L1 and L2 and subsequent surface melt from the L1 and L2 drainage basins (delineated by the vertical black line). Shaded light gray areas display periods categorized as short-lived speedup events (S4 and S5).

up glacier via longitudinal stresses [*Nick et al.*, 2009] or (2) local changes in subglacial water pressure may initiate speed variations as observed on land-terminating margins of the GRIS [*Bartholomew et al.*, 2010].

4.1. Mechanism for Speed Variations

[19] If the observed speedups had been directly caused by changes at the calving front, we would expect the magnitude of the ice speed response to each event to decrease up glacier [*Nick et al.*, 2009] and the ice surface at KNS1 to have lowered as the ice was stretched by positive longitudinal strain rates [*Thomas*, 2004]. To examine the surface lowering which could be expected at KNS1 from an event such as S3, we obtained the speed at a point ~16 km down glacier from KNS1 prior to and after S3 from interferometric synthetic aperture radar (InSAR) data [*Joughin et al.*, 2010]. Our estimated acceleration between this point and KNS2 (a distance of ~28 km) would have produced additional longitudinal strain rates of ~+0.023 yr^{-1} at KNS1. Mean ice thickness for this region is not known, but on the basis of ice thickness for similar-sized marine-terminating outlet glaciers (e.g., ~600 m for Kangerdlugssuaq Gletscher near terminus and ~1900 m for ~30 km inland (using Center for Remote Sensing of Ice Sheets bed elevation data, https://www.cresis.ku.edu/data/greenland, and the 1 km Bamber GRIS surface DEM [*Bamber et al.*, 2001])), we employ a value of 1200 m. Using the above values of strain and ice thickness, ignoring any changes in ice thickness advection, and assuming that the cause of S3 originated at the calving front, we estimate that lowering rates at KNS1 would be approximately 0.13 m d^{-1} (0.054 m d^{-1} for 500 m ice thickness and 0.16 m d^{-1} for 1500 m ice thickness) [*Thomas*, 2004]. On the contrary, we observed synchronous vertical *uplift* at KNS1 during S3 of ~+0.03 m d^{-1} (Figure 3a), indicating that the speedup did not originate at the calving front.

[20] Uplift was also recorded at KNS1 during S2–S6, none of which coincided with major changes (i.e., visible in the time-lapse photographs) at the calving terminus. Furthermore, if the speedups measured across sites KNS1–KNS4 were all caused by perturbations at the calving front, we would expect KNS1 to display the greatest ice flow response to each event and the relative magnitude of each acceleration to decrease with distance up glacier [*Nick et al.*, 2009]. Instead, our data show that the maximum relative acceleration during each event occurred at sites farther up glacier as the melt season progressed, indicating a local cause. Although the arrival of the turbid plume at the terminus could also have affected the glacier's force balance by removing the ice mélange (which may inhibit calving [*Amundson et al.*, 2010]), it occurred after S3, suggesting that it was a consequence rather than a cause of the speedup and lake drainage observed farther up glacier. This indicates that there was no coupling between the terminus and KNS1 (36 km apart) at this stage of the melt season [cf. *Kamb and Echelmeyer*, 1986] and that the breakup of the ice mélange had little effect on ice flow. This lack of coupling between the terminus and ice ~36 km up glacier is in line with the observations of *Thomas et al.* [2009], who reported dynamic thinning of >10 m yr^{-1} between 1998 and 2001 within 10 km of the terminus decreasing to zero ~30 km inland.

[21] During each speedup event at KNS1, maximum horizontal speed coincided with maximum uplift rate. Such behavior is consistent with enhanced basal sliding as a consequence of high basal water pressures [*Iken et al.*, 1983; *Iken*, 1981]. The asymmetrical shape of the uplift and subsidence (steep uplift and more gradual subsidence) is also indicative of subglacial water pressure forcing and has been attributed to the (relatively) slow release of basal water trapped in cavities following the cessation of increased surface meltwater input [*Iken et al.*, 1983]. This "hydraulic jacking" has been well documented on temperate glaciers [*Iken et al.*, 1983; *Iken*, 1981; *Iken and Bindschadler*, 1986; *Mair et al.*, 2003] and has also been observed previously on the GRIS [*Zwally et al.*, 2002; *Das et al.*, 2008; *Shepherd et al.*, 2009; *Bartholomew et al.*, 2010].

[22] Further evidence for local hydrological forcing at KNS1 comes from temporal patterns of measured surface melt and lake drainage discharge (which we use as a proxy for water input to the subglacial system). Although surface

meltwater will initially percolate and refreeze in the snowpack, eventually the snowpack temperature reaches the pressure melting point and becomes saturated [*Pfeffer et al.*, 1991]. Once this occurs, surface meltwater can rapidly access the ice bed via existing moulins [*Catania and Neumann*, 2010] and crevasses and influence basal sliding. This is likely to have been the cause of S1 and S2 at KNS1 as both followed several days of above-freezing temperatures and consequent increased melt (Figures 3a–3e). The coincidence of other speedups (e.g., S3 and S4) with reductions in lake volume is strong evidence that they were caused by these lakes draining to the glacier bed. It is likely that these large volumes of meltwater were initially input to an inefficient distributed drainage system, creating episodes of high subglacial water pressure, hydraulic jacking, and enhanced basal sliding. Expansion of the efficient channelized subglacial system therefore follows up-glacier development of surface melting, lake formation, and hydrofracture and proceeds in a series of steps as new ice-bed connections are established [*Nienow et al.*, 1998].

4.2. Coupling of Ice Flow Over ~10 km

[23] At KNS2–KNS4 we observed speedups with different simultaneous patterns of surface uplift from those observed at KNS1 (Figures 3b–3d). For example, during S3 at KNS1 we observed vertical uplift of 0.14 m, while at KNS2 the ice surface lowered simultaneously by ~0.02 m. Indeed, we estimate surface lowering at KNS2 resulting from the relative accelerations at KNS1 and KNS3 during S3 (i.e., due to the additional horizontal strain imposed by the speedup event) to be ~0.02 m d^{-1}. Theoretical and field studies show that the stress coupling length, L, should range between 4 and 10 times the ice thickness (approximately 4 to >10 km along our transect) depending on glacier geometry and bed topography [*Balise and Raymond*, 1985; *Kamb and Echelmeyer*, 1986]. L is therefore comparable to the distance between our GPS sites, indicating that speedups could have resulted from longitudinal or lateral coupling to adjacent hydraulically induced faster flowing ice [*Price et al.*, 2008]. We note, however, that although S2 is observed at KNS2, S1 is not, and neither S1 nor S2 are measured at KNS3. The former suggests that longitudinal stress coupling over ~10 km is not possible until the bed is primed, for example, once basal water pressure has reached a critical proportion of overburden pressure [*Pimentel and Flowers*, 2010], while the latter indicates that sites ~20 km apart are not stress coupled.

[24] The coincidence of S4 at KNS1 and KNS2 with drainage of nearby lakes (Figure 5) suggests that this speedup was due to local coupling to areas of hydromechanical forcing. Simple modeling of subglacial channel expansion and closure (following *Spring and Hutter* [1981]; see auxiliary material)[1] suggests that the drainage of L1 and L2 (Figures 5b and 5c) would be sufficient to open large (~18 m^2) conduits at the bed and that water pressures within these channels would exceed ice overburden pressure for longer than 24 h. Thick overlying ice could reduce conduit diameter in less than a day, but the conduits would remain open because of surface melt–derived discharge assumed to reach the bed via moulins at the lake drainage sites [e.g., *Das et al.*, 2008]. A subsequent increase in discharge to the ice bed on day 213 (Figures 5b and 5c), caused by the drainage of several lakes between 1600 and 2000 m, would have been sufficient to increase basal water pressures above ice overburden pressure once again for a further 12 h during S5. This simple modeling approach produces qualitatively similar results to other simulations of supraglacial lake drainage such as those of *Pimentel and Flowers* [2010]. Supraglacial lake development is therefore important, because it provides sufficient water both to force hydrofracture through thick cold ice and to open efficient channels at the ice bed, forming a rapid surface-bed route for subsequent surface meltwater.

4.3. Slowdown Events

[25] At KNS1, following S3 and S4, horizontal speed decreased to values consistently lower than those immediately prior to the speedups. For S4 these values were also >6% below background speed. These "extra slowdowns" [*Meier et al.*, 1994] are probably the consequence of enlargement of the basal water conduits following increased surface water input. Less significant extra slowdowns are also observed at land-terminating margins [e.g., *Bartholomew et al.*, 2010]. Larger channels subsequently require greater water flux to become pressurized so that the basal resistance required to balance the driving stress can be achieved at lower speeds [*Meier et al.*, 1994]. The extra slowdowns that follow many of the later speedup events and the late season below-background speeds at each site therefore suggest that toward the end of our survey period an efficient subglacial drainage system had developed at distances of up to 48 km from the terminus [*Mair et al.*, 2002; *Anderson et al.*, 2004]. This reasoning is consistent with the findings of *Howat et al.* [2010], although slowdowns at our sites are relatively smaller, between 1% and 10% as opposed to 40% and 60%. We find that although establishment of an efficient drainage system reduces the sensitivity of the subglacial hydrological system to further meltwater inputs, it does not preclude subsequent speedups. This is demonstrated by the occurrence of S5 and S6 at KNS1 despite preceding extra slowdowns. The amount by which sensitivity is reduced depends on the balance between channel closure rates and basal water flux following channelization [*Pimentel and Flowers*, 2010; *Schoof*, 2010].

[26] The emergence of the large turbid fjord plume at the KNS calving front on day 195, indicative of the arrival of an efficient channelized subglacial system and consequent flushing of stored basal water and sediment [*Kamb et al.*, 1985], coincided with the slowdown at KNS1 after S3 (Figure 3a) and followed by less than 24 h reductions in lake area between 1200 and 1400 m (Figure 3f). A similar coincidence between ice deceleration and discharge from the basal water system was observed following the surge of Variegated Glacier, Alaska [*Kamb et al.*, 1985], and further supports a hydrological forcing mechanism for S3.

5. Conclusion

[27] Our data show that beyond 36 km up glacier of the terminus of Kangiata Nunata Sermia, a large marine-terminating outlet glacier in southwest Greenland, both seasonal and shorter-term ice flow variations are principally

[1] Auxiliary material files are available in the HTML. doi:10.1029/2010JF001948.

Table 2. The Net Effect of Seasonal Ice Flow Variations (Summer Speedup and Extra Slowdowns) on Annual Ice Speed for KNS1–KNS4[a]

	Defined Background Speed (m yr^{-1})	Mean Summer Speed (m yr^{-1})	Summer Versus Winter Percentage Difference	Percentage Annual Speed Change
KNS1	382	396	+3.7	+0.7
KNS2	216	226	+4.2	+0.9
KNS3	173	180	+3.7	+0.5
KNS4	97	99	+2.1	+0.3

[a]The summer period begins on day 155 for KNS1 and KNS2 and on day 180 for KNS3 and KNS4 and finishes at the end of our survey at each site. Ice speed for all nonsummer days is prescribed as the defined background speed.

controlled by local hydromechanical forcing rather than by changes at the calving front. At our transect, as has been demonstrated for land-terminating margins [e.g., *Bartholomew et al.*, 2010], surface melt forcing drives evolution of the subglacial drainage system, leading to uplift, acceleration, and subsequent slowdown following the establishment of an efficient channelized hydrological system [*Bartholomaus et al.*, 2008; *Das et al.*, 2008]. Lake drainages play a key role in forcing subglacial drainage evolution and often coincide with the largest speedup events. Our data support the conclusion that lakes provide sufficient accumulations of surface water to (1) force hydrofracture through thick cold ice, (2) pressurize the existing drainage system, and (3) develop efficient subglacial channels which reduce the sensitivity of the subglacial hydrological system to subsequent variations in meltwater flux. More generally, our data support previous observations [e.g., *Fudge et al.*, 2009] and modeling [e.g., *Schoof*, 2010] demonstrating that it is rapid variations in the meltwater supply to the subglacial drainage system that have the greatest effect on ice flow. In this sense, at distances >36 km from the calving front, KNS behaves similarly to other smaller glaciers elsewhere [*Iken*, 1981; *Kamb et al.*, 1994].

[28] However, as has been previously reported at locations closer to the margins of other marine-terminating glaciers [*Joughin et al.*, 2008a], the overall effect of observed seasonal flow variations on the annual motion of KNS is small compared to those reported for land-terminating glaciers [*Bartholomew et al.*, 2010] (Table 2). This in part is because the speedups are compensated for by slowdowns beneath background speed associated with the establishment of an efficient subglacial drainage system, which are greater than those reported at land-terminating margins. The short-lived speedups at KNS are also relatively small compared to those observed at land-terminating margins (up to 40% rather than 220% [*Bartholomew et al.*, 2010]). Fast flowing outlet glaciers, such as KNS, may be less sensitive to seasonal variations in surface meltwater input because basal shear heating already provides a supply of subglacial water that could maintain relatively high basal water pressures [*Joughin et al.*, 2008a] if the subglacial drainage system remains inefficient. Marine-terminating outlet glaciers tend to be deep and narrow so that lateral shear stress is likely to provide a greater proportion of the total resistance to ice flow, and changes in basal friction will have relatively less impact on ice speed [*Joughin et al.*, 2008a]. It is important to note, however, that our most down-glacier site (KNS1) is at a similar elevation to the most up-glacier site reported by *Bartholomew et al.* [2010], where the effect on annual ice speed of seasonal variations was 6%. Our results suggest that despite the above differences, sufficiently far inland from the calving front, the ice flow response of a large GRIS marine-terminating outlet glacier to variations in surface melting is similar to that of land-terminating outlet glaciers.

[29] **Acknowledgments.** We thank Tim Bartholomaus, two anonymous reviewers, and the Associate Editor for constructive comments that improved the paper. We thank U.K. Natural Environment Research Council (NERC, through a studentship to I.D.B. and grants to P.W.N., D.W.F.M., and M.A.K) and the Edinburgh University Moss Centenary Scholarship (I.D.B.) for financial support. M.A.K. was also funded by a RCUK academic fellowship. GPS equipment and training were provided by the NERC Geophysical Equipment Facility.

References

Amundson, J., M. Fahnestock, M. Truffer, J. Brown, M. Luthi, and R. Motyka (2010), Ice melange dynamics and implications for terminus stability, Jakobshavn Isbrae, Greenland, *J. Geophys. Res.*, *115*, F01005, doi:10.1029/2009JF001405.

Andersen, M. L., et al. (2010), Spatial and temporal melt variability at Helheim Glacier, east Greenland, and its effect on ice dynamics, *J. Geophys. Res.*, *115*, F04041, doi:10.1029/2010JF001760.

Anderson, R., S. Anderson, K. MacGregor, E. Waddington, S. O'Neel, C. Riihimaki, and M. Loso (2004), Strong feedbacks between hydrology and sliding of a small alpine glacier, *J. Geophys. Res.*, *109*, F03005, doi:10.1029/2004JF000120.

Balise, M., and C. Raymond (1985), Transfer of basal sliding variations to the surface of a linearly viscous glacier, *J. Glaciol.*, *31*, 308–318.

Bamber, J., S. Ekholm, and W. Krabill (2001), A new, high-resolution digital elevation model of Greenland fully validated with airborne laser altimeter data, *J. Geophys. Res.*, *106*, 6733–6745.

Bartholomaus, T. C., R. S. Anderson, and S. P. Anderson (2008), Response of glacier basal motion to transient water storage, *Nat. Geosci.*, *1*, 33–37.

Bartholomew, I., P. Nienow, D. Mair, A. Hubbard, M. King, and A. Sole (2010), Seasonal evolution of subglacial drainage and acceleration in a Greenland outlet glacier, *Nat. Geosci.*, *3*, 408–411, doi:10.1038/NGEO863.

Box, J., and K. Ski (2007), Remote sounding of Greenland supraglacial melt lakes: Implications for subglacial hydraulics, *J. Glaciol.*, *53*, 257–265.

Catania, G., and T. Neumann (2010), Persistent englacial drainage features in the Greenland Ice Sheet, *Geophys. Res. Lett.*, *37*, L02501, doi:10.1029/2009GL041108.

Chen, G. (1998), GPS kinematic positioning for the airborne laser altimetry at Long Valley, California, Ph.D. thesis, Mass. Inst. of Technol., Cambridge.

Das, S. B., I. Joughin, M. Behn, I. Howat, M. A. King, D. Lizarralde, and M. P. Bhatia (2008), Fracture propagation to the base of the Greenland Ice Sheet during supraglacial lake drainage, *Science*, *320*, 778–781, doi:10.1126/science.1153360.

Echelmeyer, K., and W. Harrison (1990), Jakobshavn Isbrae, west Greenland, seasonal variations in velocity—Or lack thereof, *J. Glaciol.*, *36*, 82–88.

Fudge, T., J. Harper, N. Humphrey, and W. Pfeffer (2009), Rapid glacier sliding, reverse ice motion and subglacial water pressure during an autumn rainstorm, *Ann. Glaciol.*, *50*, 101–108.

Gumley, L., J. Descloitres, and J. Schmaltz (2007), Creating reprojected MODIS true color images: A tutorial, version 1.0.1, Univ. of Wis.-Madison, Madison.

Herring, T., R. King, and S. McClusky (2010), Documentation for the GAMIT GPS analysis software, version 10.3, Mass. Inst. of Technol., Cambridge.

Howat, I., I. Joughin, S. Tulaczyk, and S. Gogineni (2005), Rapid retreat and acceleration of Helheim Glacier, east Greenland, *Geophys. Res. Lett.*, *32*, L22502, doi:10.1029/2005GL024737.

Howat, I., I. Joughin, and T. Scambos (2007), Rapid changes in ice discharge from Greenland outlet glaciers, *Science*, *315*, 1559–1561, doi:10.1126/science.1138478.

Howat, I., J. Box, Y. Ahn, A. Herrington, and E. McFadden (2010), Seasonal variability in the dynamics of marine-terminating outlet glaciers in Greenland, *J. Glaciol.*, *56*, 601–613.

Howat, I. M., S. Tulaczyk, E. Waddington, and H. Björnsson (2008), Dynamic controls on glacier basal motion inferred from surface ice motion, *J. Geophys. Res.*, *113*, F03015, doi:10.1029/2007JF000925.

Huybrechts, P., J. Gregory, I. Janssens, and M. Wild (2004), Modelling Antarctic and Greenland volume changes during the 20th and 21st centuries forced by GCM time slice integrations, *Global Planet. Change*, *42*, 83–105.

Iken, A. (1981), The effect of the subglacial water pressure on the sliding velocity of a glacier in an idealized numerical model, *J. Glaciol.*, *27*, 407–421.

Iken, A., and R. A. Bindschadler (1986), Combined measurements of subglacial water pressure and surface velocity of Findelengletscher, Switzerland: Conclusions about drainage system and sliding mechanism, *J. Glaciol.*, *32*, 101–119.

Iken, A., H. Rothlisberger, A. Flotron, and W. Haeberli (1983), The uplift of Unteraargletscher at the beginning of the melt season—A consequence of water storage at the bed?, *J. Glaciol.*, *29*, 28–47.

Joughin, I., S. Tulaczyk, M. Fahnestock, and R. Kwok (1996), A mini surge on the Ryder Glacier, Greenland, observed by satellite radar interferometry, *Science*, *274*, 228–230.

Joughin, I., S. Das, M. King, B. Smith, I. Howat, and T. Moon (2008a), Seasonal speedup along the western flank of the Greenland Ice Sheet, *Science*, *320*, 781–783, doi:10.1126/science.1153288.

Joughin, I., I. Howat, M. Fahnestock, B. Smith, W. Krabill, R. Alley, H. Stern, and M. Truffer (2008b), Continued evolution of Jakobshavn Isbrae following its rapid speedup, *J. Geophys. Res.*, *113*, F04006, doi:10.1029/2008JF001023.

Joughin, I., B. Smith, I. Howat, T. Scambos, and T. Moon (2010), Greenland flow variability from ice-sheet-wide velocity mapping, *J. Glaciol.*, *56*, 415–430.

Kamb, B. (1987), Glacier surge mechanism based on linked cavity configuration of the basal water conduit system, *J. Geophys. Res.*, *92*, 9083–9100.

Kamb, B., and K. A. Echelmeyer (1986), Stress-gradient coupling in glacier flow: 1. Longitudinal averaging of the influence of ice thickness and surface slope, *J. Glaciol.*, *32*, 267–298.

Kamb, B., C. Raymond, W. Harrison, H. Engelhardt, K. Echelmeyer, N. Humphrey, M. Brugman, and T. Pfeffer (1985), Glacier surge mechanism: 1982–1983 surge of Variegated Glacier, Alaska, *Science*, *227*, 469–479.

Kamb, B., H. Engelhardt, M. Fahenstock, N. Humphrey, M. Meier, and D. Stone (1994), Mechanical and hydrologic basis for the rapid motion of a large tidewater glacier: 2. Interpretation, *J. Geophys. Res.*, *99*, 14,231–15,244.

King, M. (2004), Rigorous GPS data-processing strategies for glaciological applications, *J. Glaciol.*, *50*, 601–607.

Krawczynski, M., M. Behn, S. Das, and I. Joughin (2009), Constraints on the lake volume required for hydro-fracture through ice sheets, *Geophys. Res. Lett.*, *36*, L10501, doi:10.1029/2008GL036765.

Lemke, P., et al. (2007), Observations: Changes in snow, ice and frozen ground, in *Climate Change 2007: The Physical Science Basis. Contribution of Working Group I to the Fourth Assessment Report of the Intergovernmental Panel on Climate Change*, edited by S. Solomon et al., chap. 4, pp. 337–384, Cambridge Univ. Press, New York.

Luckman, A., and T. Murray (2005), Seasonal variation in velocity before retreat of Jakobshavn Isbrae, Greenland, *Geophys. Res. Lett.*, *32*, L08501, doi:10.1029/2005GL022519.

Mair, D., P. Nienow, M. Sharp, T. Wohlleben, and I. Willis (2002), Influence of subglacial drainage system evolution on glacier surface motion: Haut Glacier d'Arolla, Switzerland, *J. Geophys. Res.*, *107*(B8), 2175, doi:10.1029/2001JB000514.

Mair, D., I. Willis, U. Fischer, B. Hubbard, P. Nienow, and A. Hubbard (2003), Hydrological controls on patterns of surface, internal and basal motion during three "spring events": Haut Glacier d'Arolla, Switerland, *J. Glaciol.*, *49*, 555–567.

Meier, M., S. Lundstrom, D. Stone, B. Kamb, H. Engelhardt, N. Humphrey, W. W. Dunlap, M. Fahnestock, R. M. Krimmel, and R. Walters (1994), Mechanical and hydrologic basis for the rapid motion of a large tidewater glacier: 1. Observations, *J. Geophys. Res.*, *99*, 15,219–15,229.

Moon, T., and I. Joughin (2008), Changes in ice front position on Greenland's outlet glaciers from 1992 to 2007, *J. Geophys. Res.*, *113*, F02022, doi:10.1029/2007JF000927.

Nick, F., A. Vieli, I. Howat, and I. Joughin (2009), Large-scale changes in Greenland outlet glacier dynamics triggered at the terminus, *Nat. Geosci.*, *2*, 110–114, doi:10.1038/ngeo394.

Nienow, P., M. Sharp, and I. Willis (1998), Seasonal changes in the morphology of the subglacial drainage system, Haut Glacier d'Arolla, Switzerland, *Earth Surf. Processes Landforms*, *23*, 825–843.

O'Neel, S., K. Echelmeyer, and R. Motyka (2001), Short-term flow dynamics of a retreating tidewater glacier: LeConte Glacier, Alaska, U.S.A., *J. Glaciol.*, *47*, 567–578.

Parizek, B., and R. Alley (2004), Implications of increased Greenland surface melt under global-warming scenarios: Ice sheet simulations, *Quat. Sci. Rev.*, *23*, 1013–1027.

Parry, V., P. Nienow, D. Mair, J. Scott, B. Hubbard, K. Steffen, and D. Wingham (2007), Investigations of meltwater refreezing and density variations in the snowpack and firn within the percolation zone of the Greenland Ice Sheet, *Ann. Glaciol.*, *46*, 61–68.

Pfeffer, W., M. Meier, and T. Illangasekare (1991), Retention of Greenland runoff by refreezing: Implications for projected future sea level change, *J. Geophys. Res.*, *96*, 22,117–22,124.

Pimentel, S., and G. Flowers (2010), A numerical study of hydrologically driven glacier dynamics and subglacial flooding, *Proc. R. Soc. A*, *467*, 537–558, doi:10.1098/rspa.2010.0211.

Price, S., A. Payne, G. Catania, and T. Neumann (2008), Seasonal acceleration of inland ice via longitudinal coupling to marginal ice, *J. Glaciol.*, *54*, 213–219.

Pritchard, H., R. Arthern, D. Vaughan, and L. Edwards (2009), Extensive dynamic thinning on the margins of the Greenland and Antarctic Ice Sheets, *Nature*, *461*, 971–975, doi:10.1038/nature08471.

Rignot, E., and P. Kanagaratnam (2006), Changes in the velocity structure of the Greenland Ice Sheet, *Science*, *311*, 986–990, doi:10.1126/science.1121381.

Rignot, E., J. Box, E. Burgess, and E. Hanna (2008), Mass balance of the Greenland Ice Sheet from 1958 to 2007, *Geophys. Res. Lett.*, *35*, L20502, doi:10.1029/2008GL035417.

Schoof, C. (2010), Ice-sheet acceleration driven by melt supply variability, *Nature*, *468*, 803–806, doi:10.1038/nature09618.

Shepherd, A., and D. Wingham (2007), Recent sea-level contributions of the Antarctic and Greenland Ice Sheets, *Science*, *315*, 1529–1532, doi:10.1126/science.1136776.

Shepherd, A., A. Hubbard, P. Nienow, M. King, M. McMillan, and I. Joughin (2009), Greenland Ice Sheet motion coupled with daily melting in late summer, *Geophys. Res. Lett.*, *36*, L01501, doi:10.1029/2008GL035758.

Shreve, R. (1972), Movement of water in glaciers, *J. Glaciol.*, *11*, 205–214.

Sneed, W. A., and G. S. Hamilton (2007), Evolution of melt pond volume on the surface of the Greenland Ice Sheet, *Geophys. Res. Lett.*, *34*, L03501, doi:10.1029/2006GL028697.

Spring, U., and K. Hutter (1981), Numerical studies of jökulhlaups, *Cold Reg. Sci. Technol.*, *4*, 227–244.

Sundal, A., A. Shepherd, P. Nienow, E. Hanna, S. Palmer, and P. Huybrechts (2009), Evolution of supra-glacial lakes across the Greenland Ice Sheet, *Remote Sens. Environ.*, *113*, 2164–2171.

Tedesco, M. (2007), Snowmelt over the Greenland and Antarctica Ice Sheets from spaceborne radiometric data: Extreme events and updated trends, *Geophys. Res. Lett.*, *34*, L02504, doi:10.1029/2006GL028466.

Tedesco, M., M. Serreze, and X. Fettweis (2008), Diagnosing the extreme surface melt event over southwestern Greenland in 2007, *Cryosphere*, *2*, 159–166.

Thomas, R. (2004), Force-perturbation analysis of recent thinning and acceleration of Jakobshavn Isbrae, Greenland, *J. Glaciol.*, *50*, 57–66.

Thomas, R., E. Frederick, W. Krabill, S. Manizade, and C. Martin (2009), Recent changes on Greenland outlet glaciers, *J. Glaciol.*, *55*, 147–162.

van de Wal, R., W. Boot, M. van den Broeke, C. Smeets, C. Reijmer, J. Donker, and J. Oerlemans (2008), Large and rapid melt-induced velocity changes in the ablation zone of the Greenland Ice Sheet, *Science*, *321*, 111–113, doi:10.1126/science.1158540.

van den Broeke, M., J. Bamber, J. Ettema, E. Rignot, E. Schrama, W. J. van de Berg, E. van Meijgaard, I. Velicogna, and B. Wouters (2009), Partitioning recent Greenland mass loss, *Science*, *326*, 984–986, doi:10.1126/science.1178176.

van der Veen, C. J. (2007), Fracture propagation as means of rapidly transferring surface meltwater to the base of glaciers, *Geophys. Res. Lett.*, *34*, L01501, doi:10.1029/2006GL028385.

Zwally, H., W. Abdalati, T. Herring, K. Larson, J. Saba, and K. Steffen (2002), Surface melt-induced acceleration of Greenland Ice Sheet flow, *Science*, *297*, 218–222, doi:10.1126/science.1072708.

I. D. Bartholomew, P. W. Nienow, and A. J. Sole, School of Geosciences, University of Edinburgh, Drummond Street, Edinburgh EH8 9XP, UK. (andrew.sole@ed.ac.uk)

M. J. Burke, Department of Geography, Simon Fraser University, Burnaby, BC V5A 1S6, Canada.

I. Joughin, Applied Physics Laboratory, University of Washington, 1013 NE 40th St., Seattle, WA 98105-6698, USA.

M. A. King, School of Civil Engineering and Geosciences, Newcastle University, Newcastle upon Tyne NE1 7RU, UK.

D. W. F. Mair, School of Geosciences, University of Aberdeen, Elphinstone Road, Aberdeen AB24 3UF, UK.